Engineering Journal issn: 0125-8281

Article

Finite Element Analysis-Based Pre-operative Application for Biomechanical Evaluation of a Locking Plate Used in Reconstruction After En Bloc Resection of a Stage 3 Giant Cell Tumor of the Distal Radius

Wares Chancharoen[a], Saran Seehanam[b], Thanapon Chobpenthai[c], Todsaporn Fuangrod[d], and Chavin Jongwannasiri[e,*]

Laboratory of Artificial Intelligence and Innovation in Medicine (AIIM), Princess Srisavangavadhana Faculty of Medicine, Chulabhorn Royal Academy, 906 Kamphaeng Phet 6 Rd, Talat Bang Khen, Lak Si, Bangkok 10210, Thailand
E-mail: [a]wares.cha@cra.ac.th, [b]saran.hch@gmail.com, [c]thanapon.cho@cra.ac.th, [d]todsaporn.fua@cra.ac.th, [e,*]chavin.jon@cra.ac.th (Corresponding author)

Abstract. The subject of the study was a pre-operative application involving the use of a locking plate in reconstruction after en bloc resection of a Stage 3 giant cell tumor from the distal radius in a 60-year-old male patient. The essence of the application was the use of finite element analysis to determine stresses in and deformations of the bone, plate, and screws. A model of the distal radius was constructed using CT data from a specific patient and the type and magnitude of the loading on the system were those experienced by the patient during the post-surgery period. The boundary conditions used were consistent with the aforementioned loading. Several parameters were selected as adjustable parameters in the application builder toolbox. The maximum deformation of the plate was 5.05 mm. The maximum von Mises stress was 75.06 MPa in the bones and 1,123.35 MPa in the plate. A loosened screw was located at the proximal zone of the plate, with the maximum pull-out force in the screw being 679.35 N. This was comparable to the value obtained from experimental tests, thus validating the FEA results. The maximum von Mises stress in the system exceeded the yield strengths of the bones and of the plate material (Ti-6Al-4V). The proposed application may be used by orthopedic surgeons to visualize the biomechanical performance of the bones-locking plate-screws system and to guide patients for loading actions to avoid or limit in the post-surgery period.

Keywords: Distal radius, en bloc resection, locking plate, finite element analysis, pre-operative planning.

ENGINEERING JOURNAL Volume 29 Issue 2
Received 23 July 2024
Accepted 18 February 2025
Published 28 February 2025
Online at https://engj.org/
DOI:10.4186/ej.2025.29.2.93

DOI:10.4186/ej.2025.29.2.93

1. Introduction

The locking compression plate (LCP) is widely used in orthopaedic surgery for various types of fractures, including those in the distal radius. The locking compression plate is the standard plate that provides a variable length that could fit mechanical behavior around the fracture site. The advantage of the plate is that it eliminates plate-bone contact and plays a crucial role in locking the screw with the plate. The disadvantage of the plate is that the screw can only be placed perpendicular to the plate [1]. The most frequent combination is the treatment of fractures adjacent to the joint [2]. A common failure mode after distal radius locking plate surgery is screw loosening [3]. Pull-out of the screw is uncommon, with an incidence of < 0.5% of cases [4, 5]. One study has shown that bending of the fixation plate is also the cause that leads to screw loosening or pull-out [6]. Loosening tends to occur with smaller threads at the head of the screw, which leads to eventual failure due to micromotion [7]. The number of screws used in the locking plate does not significantly impact overall failure [8]. Marwan et al. reported the case of a screw loosening in a patient who suffered distal radius fracture, which caused the patient to have wrist and hand pain as well as many complications, such as restricted wrist and finger movement [9].

In orthopaedic surgery, pre-operative planning aims to create the best surgical result while ensuring limb functionality of a patient [10, 11]. There are many pre-operative planning methods. Da Silva et al. performed cranial surgery to treat cranial nerve, which included pre-operative surgery using anatomical landmarks before creating a 3D model of the skull. Afterward, the model was studied before performing surgery on the patient [12]. In the treatment of comminuted distal radius fractures, Özbek et al. found that the intra-operative skyline method resulted in small amount of dorsal screw penetration [13]. Yoshii et al. suggested pre-operative planning for distal radius fracture treatment. By performing a pre-operative CT scan of the injured wrist, a 3D image was created. The dimensional coordinate of the fixation plate and the radius bone were marked and used as reference points [14]. Mathews et al. suggested used pre-operative radiographs for patients who opted for surgical correction of distal radius fracture [15].

Moreover, the finite element analysis (FEA) method has been used in many pre-operative planning procedures. Ruggiero et al. performed a pre-operative examination of the patient with temporal hollowing. FEA was used for implant optimization [16]. Reggiani et al. used FEA to find the model with suitable stability for the pre-operative session. The model of the cadaveric femur was generated from a CT scan before simulating it in the pre-operative software. The FEA results were validated using results from experimental tests [17]. For surgical treatment of diaphyseal tibia fractures, Travascio et al. reported that computational modeling could improve the development of implant and screw design for enhancement the bone healing [18].

Although FEA is useful in pre-operative planning, its complexity in setting up conditions and applying loads makes it difficult for surgeons to use directly. To address this, we developed a simplified application where surgeons only need to input basic parameters and run simulations, making FEA more accessible and user-friendly for medical use.

The purpose of the present study was to develop an FEA-based pre-operative application to investigate the biomechanical properties of the bones and a distal radius locking plate system (plate and screws) used in this study involved the en bloc resection of a Campanacci Grade 3 primary aggressive giant cell tumor of the distal radius, a challenging tumor type due to its high recurrence potential and aggressive nature. We limited the application to one patient (60-year-old man) in which the reconstruction involved placement of a vascularized ulnar graft, using the locking plate. Thus, the screws on the plate were used to secure the plate between the proximal radius and the graft. A 3D model of the bones-plate-screws system was constructed using CT data from the patient. For the FEA, a commercially available software package (COMSOL Multiphysics) was used. Several parameters relevant to the clinical case were chosen as adjustable parameters in the developed COMSOL application. FEA was used to determine von Mises stresses, deformations, and stress tensors in each of the bones and the screws. Some of the FEA results were validated using results from an experimental test.

2. Materials and Methods

The workflow of the development of the application via the application builder function in the COMSOL Multiphysics software is presented in Fig. 1. The flowchart has three steps. The first step was modeling configuration. This process involved use of from the patient CT scan data from the patient to obtain a 3D model (Fig. 1A). The CT scans of the patient were obtained with the forearm in the pronation position. This positioning was chosen to ensure optimal visualization of the bone and surrounding structures for accurate 3D modeling. In the second step, the FEA method was used to calculate the stresses and deformations (Fig. 1B). In the third step, some of the results were validated (Fig. 1C).

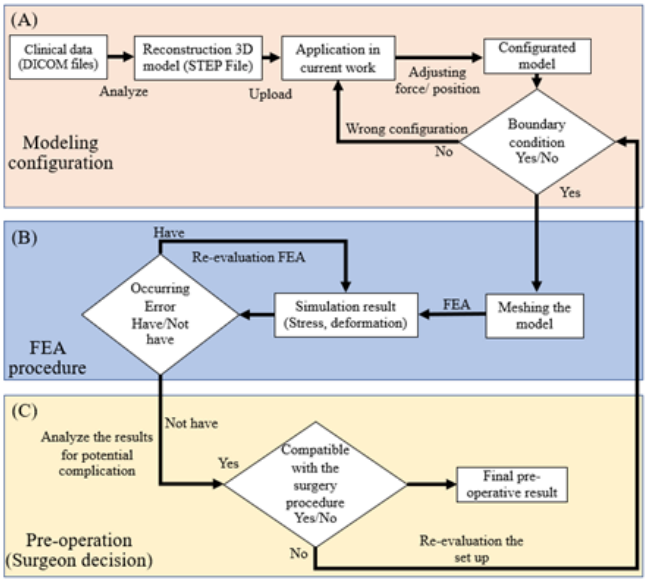

Fig. 1. The flowchart of the application procedure from the surgeon's viewpoint. (A) The workflow of the modeling configuration from DICOM files to its boundary conditions. (B) The FEA procedure, which included meshing and analysis. (C) The results were used for evaluation of biomechanical performance.

2.1. Transforming Clinical Data to 3D Model

According to Fig. 2A, the referenced clinical case in this study was the en bloc resection at the distal radius in a male patient (60-year-old man), with a resection length of 4 cm [19]. After removing the tumor, the en bloc resection reconstruction was performed using ulnar translocation along with the vascularized grafting process to replace the excised section of the distal radius. The area in the scapholunate region was cut into a large slot for the vascularized ulnar graft placement. Then cortical screws on the locking plate were used to secure the ulnar graft to the scaphoid, lunate, capitate, and proximal radius (Fig. 2A). One month after surgery, a second radiography image was taken (Fig. 2B). The image displayed a severe deformation from the vascularized ulnar graft. Another complication was that a screw at the second bottom of the locking plate had loosened from its position (see the circle in Fig. 2B). According to the surgeon's testimony, the patient's activities of daily living included lifting heavy objects, this frequent action led to loosening screw out after one month. which made the patient undergo another operation [19]. As such, it is possible to use the before-and-after data as a reference to observe the cause and effect of the failure of the implant fixation in the patient case, which led us to create a pre-operative application to predict potential failures.

The models used in the development of the application were made in SolidWorks 2023 (Dassault Systemes, France.) Models of the ulnar and radius were reconstructed from CT scan data from the patient. The CT scanned images were converted into a DICOM (digital imaging and communication) format, then rendered in the 3D Slicer. The 3D Slicer software was used to process CT scan data obtained from a SOMATOM Definition CT scanner (120 kV, 167 mA, Siemens, USA). In the 3D Slicer software, a voxel size was set to 0.8 mm x 0.8 mm x 0.8 mm, with a slice thickness of 1 mm was applied to the rendered model to smoothen bone geometry further. To improve the quality of bone density, the segmentation thresholds were set as 150 – maximum of limit thresholds. All the bone models were assembled into a single piece, with the ulnar graft connected to the scapholunate region and the proximal radius connected to the ulnar graft. For the model of the locking plate (Stryker, Corp., Mahwah, NJ, USA) the geometry of the plate was obtained by using vernier scales and recreated in the SolidWorks program. The ulnar and radius were then assembled with the plate, which was secured using 2.3 mm-diameter screws for a screw, the geometry is a cylinder without threads since it has been shown that they do not affect the global stresses in the screws and the plate. Caiti et al. showed that the local mechanical response of the interface between the bone and a screw thread does not influence the major global stresses in the screws and the plate [20]. A 4-noded tetrahedral finite element mesh was used. The sensitivity analysis was performed with mesh size between 0.75 mm and 2.5 mm (Fig. 3A-E). The von Mises stress was determined at a point between screw numbers 6 and 7 (Fig. 3F).

To serve as a pre-operative tool, the developed application must be able to simulate loading cases simulating real life movements for each surgical case, depending on the requirements of the patient and the orthopedic surgeon. In this case, the loading condition was set to be as shown in Fig. 4A; namely, bending moment and axial compressive load. The loading was applied at the distal-most region of the radius, and the radius was then fixed at its proximal-most region. These loading conditions were used to simulate the simplified use of the forearm after the surgical operation; that is, actions such as lifting objects, pushing oneself off a chair, and squeezing objects.

The aforementioned loading conditions are more complex than the simple loading case set for this case, as the bones have many muscle groups and ligaments that support the distribution of loads. The loading magnitude and position of the loading on the bones during different activities are extremely difficult to determine, as pointed out in various studies [21-24]. Therefore, in the present work, as a simplification and to serve as a general loading case for the surgeon, the developed application assumes the position of two loading types (Fig. 4A) which allows the force parameters to be changed (Fig. 4B).

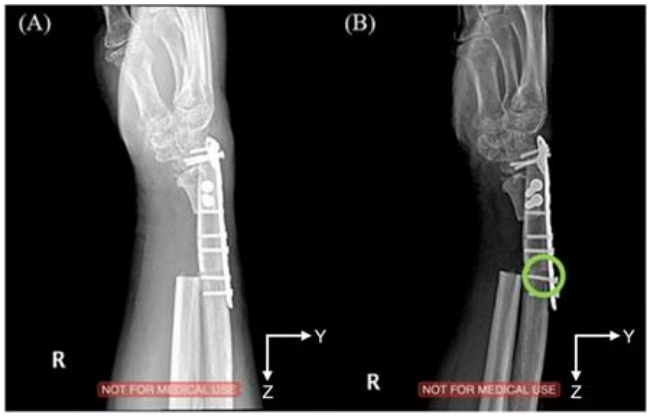

Fig. 2. (A) The radiography image after performing the surgery with the en bloc resection method on the right distal radius of a 60-year-old man. (B) The radiograph image of the deformed bone at the area of vascularized graft and a screw loosened from its position at the second bottom of the distal radius locking plate (shown marked using the green circle). The Y-axis represents the frontal axis and the pull-out axis (dorsal).

The radius, ulnar, scaphoid, and lunar bones were each assumed to have linear, homogenous, and isotropic elastic properties and were modeled to be a single solid piece instead of having separate layers of cortical and cancellous bones, as previous studies have shown that the separation between these layers has an insignificant impact on certain finite element analyses [25-26]. To allow for wider applicability, we have chosen to ignore, in particular, ligaments, muscles, and tendons. As for the mechanical properties related to the FEA of the bones, the major one is the modulus of elasticity [27]. For our analysis, as stated earlier, the material of all the bones involved are homogenous and isotropic; as such, E in each of the bones will be obtained from that of the radius, according to Bosisio et al., through the inverse-finite element method, E of the radius was found to be 16 ± 1.8 GPa. Thus, for each of the bones, we used E = 14.2 GPa, that being the lower range of the published values in the literature [28]. The locking plate and the screws were considered to be fabricated from Ti-6Al-4V. The connection between the plate and the screws was represented as a fixed union of the components. A summary of the properties of the materials used in the analysis is given in Table 1.

2.2. Configuration Parameters

According to Fig. 1A and 1B, the options from the application builder contained two main parameters. First, the conditions of the bone and the implant were adjustable according to the surgeon's requirements. Second, the application must simulate the results by using stress analysis and display biomechanical results of the bone and the implant. Therefore, to meet the surgeon's requirements, the applied forces to the model must be adjustable with respect their orientations and magnitudes depending on the physical situation of the patient. The position of the locking distal radius plate also should be relocated according to the surgeon's decision and clinical conditions (Fig. 5A). All six-degrees of freedom of the locking plate were set as adjustable parameters in the parameter setting (Fig. 5B). It also included forces from the boundary conditions from Fig. 4B. The magnitude and orientation of the force to the distal bone were obtained from physiological information [21-24]. In the input window of the application builder, all the adjustable parameters of forces and degree of movements could be changed depending on situation of patient. Therefore, these parameters appeared in the graphic user interface (GUI). highlighted with the rectangular box in Fig. 6.

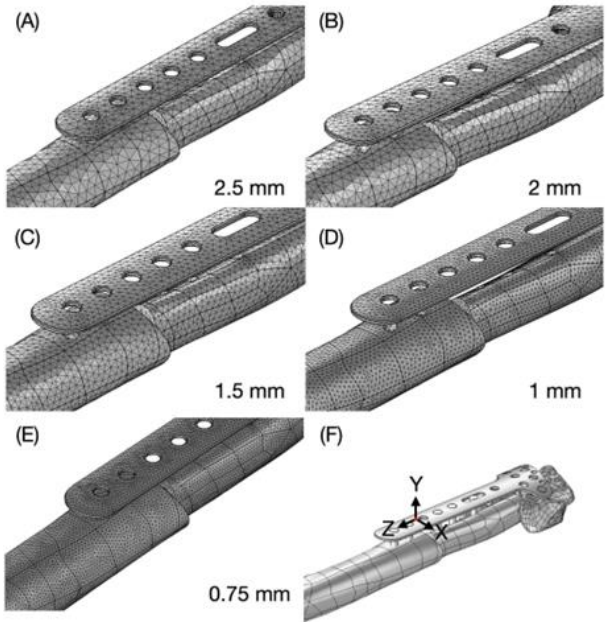

Fig. 3. The assembly of the components comprises part of the radius, ulnar, scaphoid, lunate, and capitate, and the dorsal distal radius locking plate. The mean finite element mesh size was set to (A) 2.5 mm, (B) 2 mm, (C) 1.5 mm, (D) 1 mm, (E) 0.75 mm, and (F) The von Mises stress was extracted from a point between screws No. 6 and 7.

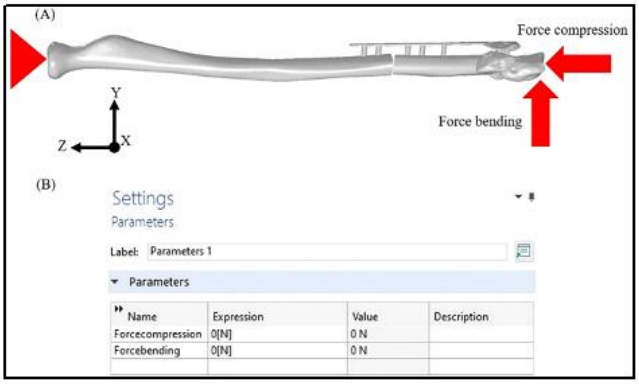

Fig. 4. (A) The FEA condition of the 3D model with force applied to the scapholunate region and the capitate (right arrows) while the fixed support was set at the end of the proximal radius (left arrow). (B) Prerequisite parameters of force set up for application in application builder function.

2.3. Output Parameters

According to Fig. 1C, the outcomes of the application were the stresses and deformations in the bones, locking plate, and screws. Moreover, we used a stress tensor to analyze the stress in each direction to better understand the biomechanics. Therefore, the stress tensor of the loosening screw indicated the prediction of the loosening probability of the screw. In this study, we applied three parameters used as the output for this simulation for analyzing the biomechanics of the bones and the plate as well as predicting the loosening of the screws.

First, the von Mises stress was used to denote the stress in a body. The von Mises stress criterion was used as the design criterion. Specifically, at any point in a given bone, the von Mises stresses should be < 150 MPa [28], and for the locking plate and the screws, it should be < 880 MPa [29].

Second, the deformation of the simulated case must be within acceptable clinical limits. For this referenced clinical case of the en bloc resection of a tumor from the distal radius, we used the American Academy of Orthopaedic Surgeons (AAOS) clinical practice guidelines on the treatment of distal radius fractures as the clinical failure criteria [30]. In the third section of these guidelines, it is stated that operative fixation is recommended for post-reduction cases in which the distal radius shortens by more than 3 mm. Thus, for the present study case, the distal radial shortening, observed under any load, should be ≤ 3 mm.

Third, the stress tensor can be used to measure the pull-out force for a screw. Zdero et al. mentioned that the highest stress which led to pull-out failure of a screw occurred along its longitudinal axis [31], which we applied in this study.

Table 1. Mechanical properties of the materials in the model.a

Radius, Ulnar bone, Scaphoid, and Lunate	
Modulus of elasticity (GPa)	14.2
Poisson's Ratio	0.3
Yield Strength (MPa)	150.0
Locking Plate and Screws (Ti-6Al-4V)	
Modulus of elasticity (GPa)	113.8
Poisson Ratio	0.34
Yield Strength (MPa)	880.0

[a]For the bones and the plate, the property values were taken from the works of [28] and [29], respectively.

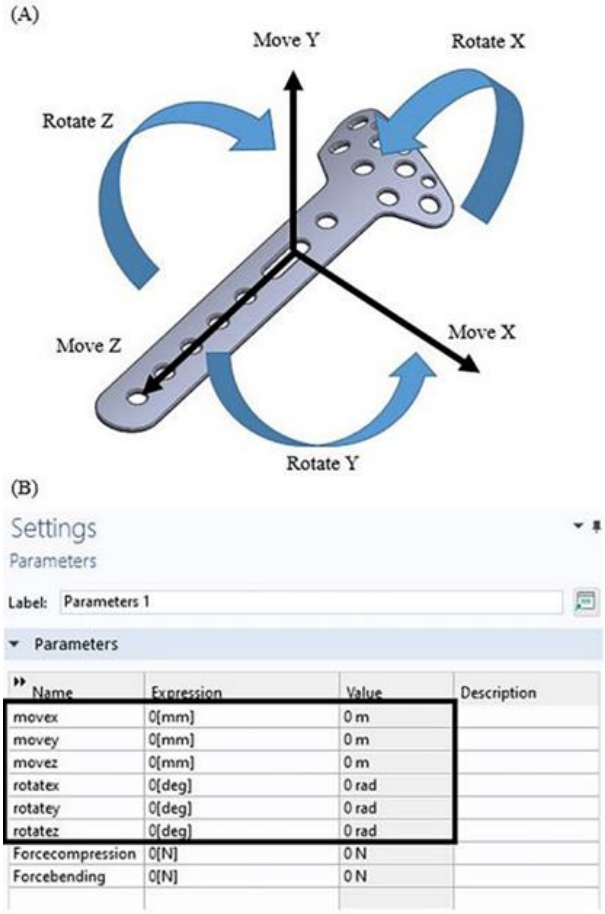

Fig. 5. (A) The six degrees of freedom of the dorsal distal radius locking plate. (B) The prerequisite parameters of all degrees of movement of the plate (highlighted with the rectangular box).

Moreover, in the application builder built-in module in COMSOL Multiphysics, we set up the command buttons from the ribbon tab. The necessary command buttons were for the geometry, obtaining the finite element mesh of the model, computation of the stresses, and the display of the results (Fig. 7A). As for the results section, the calculated stresses and deformations were selected (Fig. 7B). After selecting both command buttons and display of the results, the graphic user interface (GUI) of the developed application could be seen (Fig. 7C). All selected command buttons appeared on top of display as highlighted with the rectangular box A (Fig. 7C) and the stresses and deformations appeared at bottom left, as highlighted with the rectangular box (Fig. 7C). Some data on the example case that used the developed application are given in the Supplementary Material.

To validate the pull-out force of a screw, an experiment was carried out per the protocols given in ASTM F543-17 [32]. A photograph of the experimental set-up for determining the screw axial pull-out force is presented in Fig. 8. Specifically, a bone with an inserted screw was tested in a universal materials testing machine (ElectroPuls E10000; Instron, Inc., Norwood, MA, USA). The screw holder was mounted over the head of a screw. Specimens were tested at a crosshead deformation

DOI:10.4186/ej.2025.29.2.93

rate of 2 mm/min. The result obtained were the maximum pull-out force of the screw.

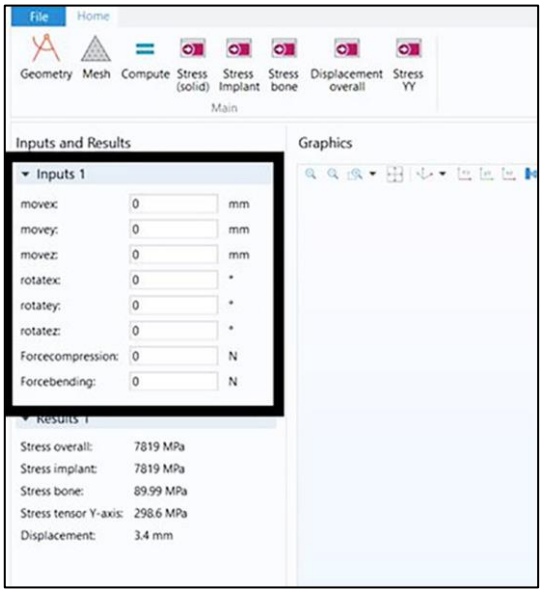

Fig. 6. The graphic user interface (GUI) of the developed application with the input window, which showed the adjustable parameters of the degree of movements and force (highlighted with the rectangular box).

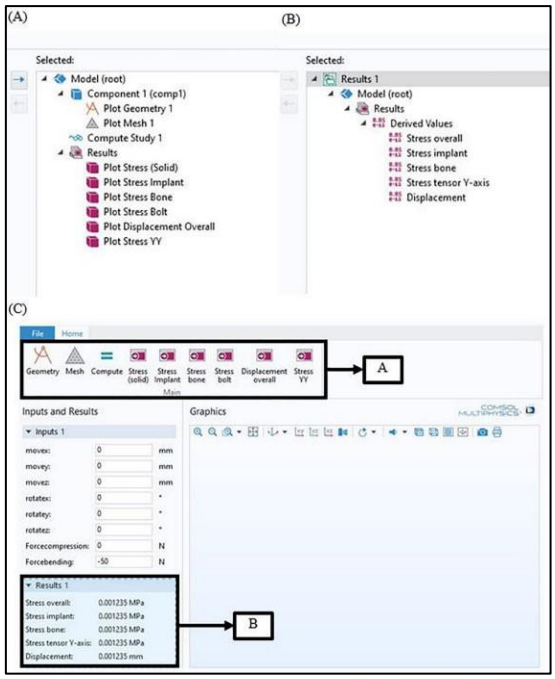

Fig. 7. (A) All command buttons for the application, showing the geometry, obtaining the finite element mesh of the model, computation steps, and results. (B) The results tab shows the stresses and deformation. (C) The final display of the graphic user interface for the developed application, with the rectangular box A showing the command buttons and the rectangular B showing the stresses and deformations.

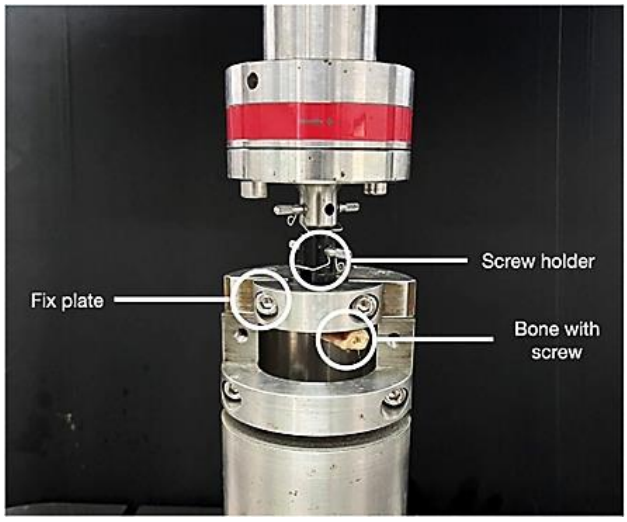

Fig. 8. Photograph of the experimental set-up used for the determination of axial pull-out force of a screw.

3. Results

3.1. Validation of Radial Shortening

According to the surgeon, the patient's occupation involved lifting heavy objects [19]. One of the questions in the questionnaire in the Institute of Work and Health (IWH)'s disability of arm shoulder and hand (DASH) guidelines [33] is whether the patient lifts heavy weights (> 5 kg). As such, in the present work, we set the loading force to be 50 N (~5 kg), applied perpendicular to the frontal plane, with the force being applied to the dorsal side of the scaphoid and the lunate. This is to replicate a loading case where the patient is pointing his/her arm forward and holding a heavy object with the palm side down. It is important to note that in reality, the force applied to the scaphoid and the lunate may not be exactly 50 N when holding onto an item weighing 5 kg. However, to simplify the simulation, and to account for cases where the patient may be lifting objects heavier than 5 kg, the assumed loading case was used.

As mentioned earlier in the expected results section, according to the clinical practice guidelines of the American Academy of Orthopaedic Surgeons (AAOS) [30], operative fixation is recommended for post-reduction cases in which the radius shortens by < 3 mm. From Fig. 9A and Fig. 9B, it can be seen that when a load of 50 N was applied, FEA gave radial shortening of 1 mm. Thus, it meets the AAOS guidelines. However, screw loosening occurred.

When comparing the simulated deformations (Fig. 9) with the actual radiography image of the distal radius fracture in the patient, similar deformations of the plate were found in both cases. Thus, we can assume that the simulated deformations can be used to predict the actual deformations.

3.2. Validation of Stress in Bones, Distal Radius Locking Plate, and Screws

A model sensitivity analysis was performed, with mean finite element meshes size of 2.5 mm, 2.0 mm, 1.5 mm, 1.0 mm, and 0.75 mm. Under the same constraints and boundary conditions, von Mises stress determined at a point between screw numbers 6 and 7 (Fig. 3F) were compared and it is seen that the stress converged when the mean mesh size was between 2.5 mm and 0.75 mm (Table 2). Thus, a mean finite element mesh size of 1.5 mm was used in this study.

We also focused on the von Mises stresses in the bones, locking plate, and screws. The maximum von Mises stresses in these entities were located at a position near the hole in a screw in the proximal section of the plate (screw No. 7), with von Mises stresses of 75.06 and 1,123 MPa, respectively (Figs. 10A and 10B). Thus, the highest stress concentration was observed at the region in which a screw loosened.

The maximum von Mises stress that occurred in the locking plate was exceeded the yield strength of Ti-6Al-4V, resulting in the deformation of the plate. As a result, von Mises stress from FEA does not match with the real situation of the radiography image from Fig. 2B since screw pull-out, rather than plate deformation, occurred. Even though the screw loosening behavior could not be explained by von Mises stress in the locking plate, it could be determined by the pull-out force of each of the screws, which will be discussed in the following section.

3.3. Validation of Stress Tensor to Loosen Screw

The stress tensor could be used to analyze the loosening of the because it could consider the direction of the force effectively. The FEA from the developed application was performed on 8 screws secured between the locking plate and the bone. The positions of the screws were defined as seen shown in Fig. 11A. Consequently, Fig. 11B illustrates the pull-out force of each screw. According to Fig. 10B, the results were extracted from the highest stress tensor aligned in the frontal plane, which is the loosening direction. The maximum pull-out forces were found for screw numbers 7 and 8, which were 679.35 N and 673.54 N, respectively. Accordingly, pull-out force was reduced at the translocated ulnar region, in screw numbers 4, 5, and 6. The pull-out force in this group were 132.58-137.34 N. The lowest pull-out force (1.56-65.62 N) was found at screw numbers 1, 2, and 3.

According to the screw axial pull-out force experiment, the maximum pull-out force was 796.56 ± 191.61 N. Sample force-versus- deformation results obtained from this experiment are presented in Appendix. The region of pull-out force is shown as the shaded area in Fig. 11B. The experimental pull-out force of screw numbers No. 7 and 8 is comparable to that obtained using FEA (Fig. 11B). It was indicated that the screw No. 7 and 8 could be loose. Hence, the developed application can be used to estimate the pull-out force of each screw and the location of a loosened screw.

The results of the biomechanics analysis in the developed application showed severe deformation of the bone (Fig. 9A and 9B). The von Mises stress results indicated deformation of locking plate (Fig. 10). Consequently, Fig. 10 showed that the loosened screw (screw number 7) required the highest pull-out force calculated from stress tensor. Hence, the results from the developed application matched those from the clinical case (Fig. 2B) Therefore, the developed application was validated.

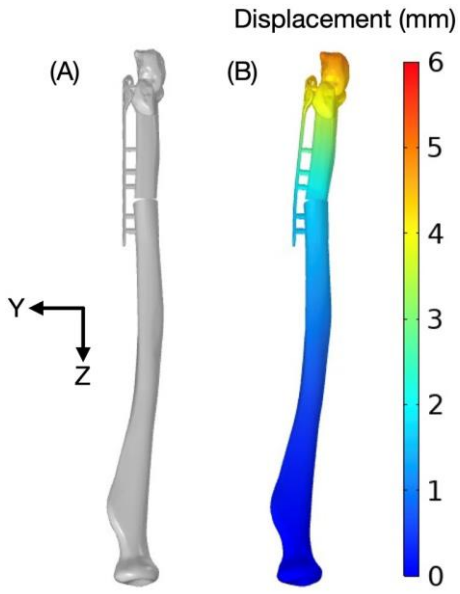

Fig. 9. The deformation contours (A) before applying the loadings and (B) after applying the loadings. The z-axis represents the proximal direction, while the y-axis represents the dorsal direction.

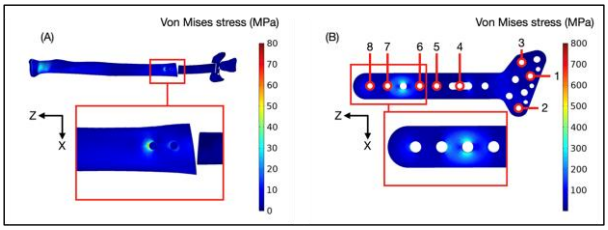

Fig. 10. von Mises stress contours of (A) the bones and (B) the locking plate. The maximum stress occurred at the bone and the locking plate at screw No. 8 hole and at a point between screws No. 6 and 7.

Table 2. Mesh sensitivity analysis of stress at a position between screw number 6 and 7.

Size	Element	Stress (MPa)	Error
2.5	58,941	227.05	-
2.0	77,732	216.27	4.7
1.5	121,966	212.71	1.6
1.0	360,289	211.71	0.4
0.75	406,609	211.45	0.1

3.4. Applicability of Application

In accordance with the ASME Verification and Validation 40-2018 Guidelines, which provides a systematic framework for generating accurate, reliable, and credible computational modeling of biomedical devices [34], the following points are made regarding the application detailed in the present work.

The "question of interest" or the objective is to predict possible failures of the clinical case, which was the assigned context of use (COU). In the risk analysis of the application, the surgeon decides "how much" the application may influence any decisions. For the validation of the sample application, in accordance with the guidelines, we added a model mesh sensitivity analysis to validate the uncertainties of the model. The results of the mesh analysis are shown in Table 2 and were discussed in the Results section.

As for the applicability of the model/developed sample application, in order to achieve the COU, which, in this case, was to predict possible failures, under specified loads, of screws at a given location on a locking plate system used in reconstruction following en bloc resection of a tumor from the dorsal distal radius, the position may be adjusted according to the translation input variable in the x-, y-, z- axes, along with the rotational input variable in the application. According to Obert et al., there is no ideal position of screws on a locking plate used to treat fracture of the distal radius [35]. As such, in our sample application, the positions of the screws on the locking plate may be changed, depending on the preference of the orthopedic surgeon. However, the orientation angle of a screw was limited to $\pm$ 5 °, which is appropriate for this clinical case; that is, the rotation ranges are within the alignment of the radius bone.

The loading forces may also be adjusted to simulate a wide range of patient actions, although the positions of the forces are fixed at the most distal part of the radius. Two loading forces of either the axial compression or tensile type (representing lifting weights and supporting oneself out of a chair) were considered in the finite element modeling [36]. Additionally, it was noted that under DASH's guidelines, a load > 5 kg was considered heavy. The present application covers those loading conditions. However, due to the nature of how the application was developed, the bones and the locking plate used in the application are patient-specific, and cannot be changed by the orthopedic surgeons directly, and must be changed by an expert in FEA.

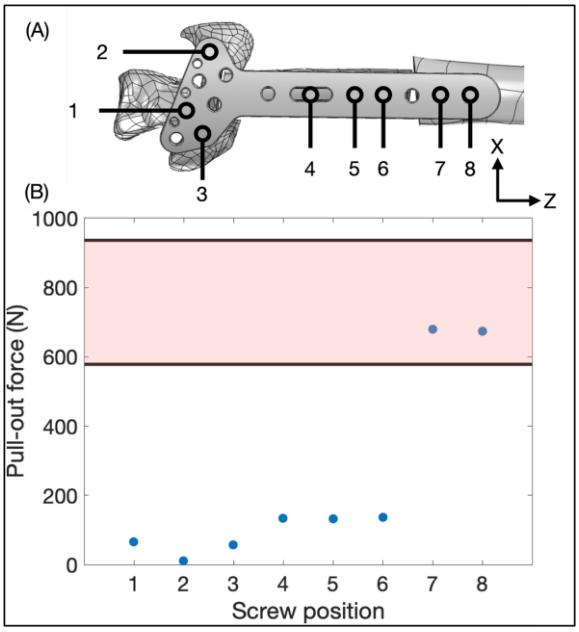

Fig. 11. A summary of the screw pull-out force results obtained using FEA (shown as the blue filled circles). (A) the definition of screw location. (B) The pull-out force of each screw. The shaded region denotes the range of screw pull-out force, obtained from experimental tests.

4. Discussion

First, the results from this application, along with the validation of the results, may only be used as a proof of concept of the developed application, and not intended to be used in medical contexts without further verification of the results via further biomechanical testing and validation with other published literature sources on similar FEA procedures. Additionally, the experimental results exhibited a standard deviation of 181 N, which corresponds to approximately 25.86% of the mean pull-out force. This relatively high variability is due to the use of real bone specimens, which inherently differ in density and structural properties. Such variability highlights the need for further biomechanical testing to better account for these differences and to improve the robustness of FEA validation.

Second, four simplifications were used in the analysis of the sample case, especially in the transformation of clinical data into the 3D models used in the analysis. These simplifications were (1) each of the bones was taken to be a homogeneous, linear and isotropic material, (2) the E was taken to be the same for all the bones, (3) the bone models were assumed to be entirely solid instead of comprising separate layers cortical and cancellous zones, and (4) the simulation of the patient lifting heavy objects may not accurately replicate actual service conditions.

While the developed application can be used to simulate loading cases for patients and may be used as a pre-operative tool, it is important to acknowledge two key limitations of the application. These are that input parameters for users are limited to only the placement of

the locking plate and the loading forces were applied in fixed positions.

For future development of FEA-based pre-operative applications, the aforementioned limitations must be addressed. Additionally, the ASME V&V 40-2018 guidelines [34] and any other relevant information must be followed in order to obtain the most accurate FEA results within the intended purpose of each clinical case or the context of the COU.

Input variables in the developed program that would make the application more realistic should be considered, an example being allowing "point and choose" placement of the locking plate. The developed application may also be developed independently instead of being developed from the COMSOL application. This would potentially allow more freedom of input, and a more robust user interface for the orthopedic surgeons who may use the developed program as a preoperative tool.

Although FEA has been used for many medical and biomechanical applications, it is important to consider possible inaccuracies that may be present in simulations of these systems [37].

The purpose of the application presented in this study is to help orthopedic surgeons to predict possible failure locations in a locking plate. Two attractive features of the application are highlighted. First, it may be used to quickly visualize the behavior of the bones, locking plate, and screws, under different loads. Second, orthopaedic surgeons may use it to guide patients on types of loading to avoid or limit during the post-surgery period.

5. Conclusions

A case study was developed and modeled using the application builder from COMSOL Multiphysics to serve as a proof of concept of an FEA-based pre-operative application. The application involved reconstruction of parts of the distal radius in a 60-year-old male patient who underwent en bloc resection of a tumor at that site. The approach presented here has many attractive features, such as the user interface is robust, easy to use, and needs only a minimal amount of input parameters for the simulation of the patient case. Key output parameters obtained from the application were stresses and deformations of the bones, locking plate, and screws. However, the model does not account for the influence of tendons and muscles, which play a crucial role in stabilizing and distributing loads. This limitation may lead to underestimations of dynamic forces and stress distributions, affecting the real-world applicability of the findings. The application may be used by surgeons to visualize locations in the locking system that may suffer failure and to guide patients as to loading activities to avoid or limit in the post-surgery period. This study demonstrates the potential of finite element analysis-based pre-operative applications in managing complex cases, such as reconstruction following en bloc resection of a Campanacci Grade 3 giant cell tumor of the distal radius.

Acknowledgements

This work was supported by Chulabhorn Royal Academy (Fundamental Fund: the fiscal year 2022 by National Science Research and Innovation Fund) [grant number: FRB650039/0240 Project code 165419]. This research project was approved by the Human Research Ethics Committee from Chulabhorn Research Institute (Code 018/2565).

We would like to express our gratitude to Pawarathe Bualert for his support in writing—original draft preparation, Pannathorn Thanyakitpaisal for his contribution to the methodology, and Warisara Boonrueng for her review, editing, and visualization.

Author Contributions

Conceptualization: C.J., T.C., T.F., and W.C.; Methodology: C.J., T.C., and W.C.; Writing—original draft preparation: S.S.; Writing—review and editing: S.S., and W.C.; Formal Analysis: S.S., and W.C; Visualization: S.S.; Data Curation: S.S., and W.C.; Supervision: C.J., T.C., T.F., and W.C.; Project administration: C.J., and W.C.; Funding acquisition: C.J., and W.C.

Appendix: Screw Pull-out Test Protocol and Sample Results

According to the screw axial pull-out force protocol described in sub-section 3.3, the maximum pull-out force was obtained for use in validating the FEA results. Three bone-screw sets were tested at a rate of 2 mm/min. Sample screw axial pull-out force versus deformation results are presented in Fig. 12.

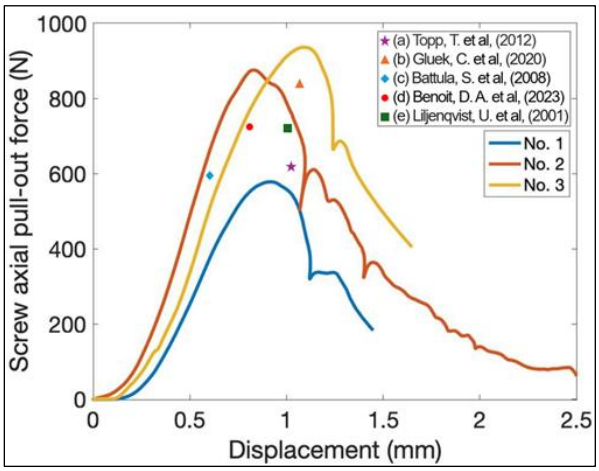

Fig. 12. Representative experimental results (No.1-3 refer to replicate tests, (a)-(e) refer to [38-42].

References

[1] D. L. Miller and T. Goswami, "A review of locking compression plate biomechanics and their advantages as internal fixators in fracture healing," *Clin Biomech*, vol. 22, no. 10, pp. 1049-1062, Dec. 2007.

[2] R. Frigg, "Locking compression plate (LCP). An osteosynthesis plate based on the dynamic compression plate and the point contact fixator (PC-Fix)," *Injury*, vol. 32, no. Suppl 2, pp. 63-66, Sep. 2001.

[3] D. Seigerman, K. Lutsky, D. Fletcher, B. Katt, M. Kwok, D. Mazur, S. Sodha, and P. K. Beredjiklian, "Complications in the management of distal radius fractures: How do we avoid them?," *Curr Rev Musculoskelet Med*, vol. 12, no. 2, pp. 204-212, Jun. 2019.

[4] R. Arora, M. Lutz, A. Hennerbichler, D. Krappinger, D. Espen, and M. Gabl, "Complications following internal fixation of unstable distal radius fracture with a palmar locking-plate," *J Orthop Trauma*, vol. 21, no. 5, pp. 316-322, May 2007.

[5] L. Zhang, M. Wang, Z. Liu, Y. Wang, Y. Sun, Z. Zhu, X. Wang, F. Liu, and Y. Cui, "Open reduction and internal fixation by volar locking plates and the "poking reduction" technique in distal radius fractures with displaced dorsal ulnar fragments: A retrospective study," *Orthop Surg*, vol. 14, no. 10, pp. 2489-2498, Oct. 2022.

[6] J. T. Capo, T. Kinchelow, K. Brooks, V. Tan, M. Manigrasso, and K. Francisco, "Biomechanical stability of four fixation constructs for distal radius fractures," *Hand*, vol. 4, no. 3, pp. 272-278, Sep. 2009.

[7] T. L. Foo, A. W. Gan, T. Soh, and W. Y. Chew, "Mechanical failure of the distal radius volar locking plate," *J Orthop Surg*, vol. 21, no. 3, pp. 332-336, Dec. 2013.

[8] D. P. Moss, K. R. Means Jr, B. G. Parks, and C. L. Forthman, "A biomechanical comparison of volar locked plating of intra-articular distal radius fractures: Use of 4 versus 7 screws for distal fixation," *J Hand Surg Am*, vol. 36, no. 12, pp. 1907-1911, Dec. 2011.

[9] Y. Marwan, A. M. Makhdom, and G. Berry, "Locking screw migration to the palm four years following surgical implantation of distal radius locking plate," *J Hand Surg Asian Pac Vol*, vol. 22, no. 3, pp. 363-365, Sep. 2017.

[10] P. Fürnstahl, G. Székely, C. Gerber, J. Hodler, J. G. Snedeker, and M. Harders, "Computer assisted reconstruction of complex proximal humerus fractures for preoperative planning," *Med Image Anal*, vol. 16, no. 3, pp. 704-720, Apr. 2012.

[11] C. Mensel, P. H. Gundtoft, and O. Brink, "Preoperative templating in orthopaedic fracture surgery: The past, present and future," *Injury*, vol. 53, no. Suppl 3, pp. S42-S46, Nov. 2022.

[12] E. B. da Silva Jr., A. G. Leal, J. B. Milano, L. F. da Silva Jr., R. S. Clemente, and R. Ramina, "Image-guided surgical planning using anatomical landmarks in the retrosigmoid approach," *Acta Neurochir*, vol. 152, no. 5, pp. 905-910, May 2010.

[13] E. A. Özbek, T. Ayanoğlu, and M. Armangil, "How effective is skyline view for avoiding dorsal cortex penetration in volar plate fixation of intra-articular and dorsal cortex comminuted distal radius fractures," *Injury*, vol. 50, no. 10, pp. 1684-1688, Oct. 2019.

[14] Y. Yoshii, T. Ogawa, A. Shigi, K. Oka, T. Murase, and T. Ishii, "Three-dimensional evaluations of preoperative planning reproducibility for the osteosynthesis of distal radius fractures," *J Orthop Surg Res*, vol. 16, no. 1, p. 131, Feb. 2021.

[15] A. L. Mathews, and K. C. Chung, "Management of complications of distal radius fractures," *Hand Clin*, vol. 31, no. 2, pp. 205-215, May 2015.

[16] F. Ruggiero, D. Dunaway, C. Budden, L. Smith, N. U. O. Jeelani, S. Schievano, J. Ong, and A. Borghi, "Finite element method for the design of implants for temporal hollowing," *JPRAS Open*, vol. 32, pp. 18-23, Dec. 2021.

[17] B. Reggiani, L. Cristofolini, E. Varini, and M. Viceconti, "Predicting the subject-specific primary stability of cementless implants during pre-operative planning: Preliminary validation of subject-specific finite-element models," *J Biomech*, vol. 40, no. 11, pp. 2552-2558, Jan. 2007.

[18] F. Travascio, L. T. Buller, E. Milne, and L. Latta, "Mechanical performance and implications on bone healing of different screw configurations for plate fixation of diaphyseal tibia fractures: A computational study," *Eur J Orthop Surg Traumatol*, vol. 31, no. 1, pp. 121-130, Jan. 2021.

[19] T. Chobpenthai, C. S. Intuwongs, S. Suvithayasiri, P. Thanindratarn, and T. Phorkhar, "En bloc resection and vascularized ulnar pedicle graft reconstruction with plate fixation for giant cell tumour of the distal radius," *J Hand Surg Eur Vol*, vol. 47, no. 5, pp. 513- 519, May 2022.

[20] G. Caiti, J. G. G. Dobbe, E. Bervoets, M. Beerens, S. D. Strackee, G. J. Strijkers, and G. J. Streekstra, "Biomechanical considerations in the design of patient-specific fixation plates for the distal radius," *Med Biol Eng Comput*, vol. 57, no. 5, pp. 1099-1107, May 2019.

[21] J. A. Pramudita, W. Hiroki, T. Yoda, and Y. Tanabe, "Variations in strain distribution at distal radius under different loading conditions," *Life*, vol. 12, no. 5, p. 740, May 2022.

[22] R. Patterson, and S. F. Viegas, "Biomechanics of the wrist," *J Hand Ther*, vol. 8, no. 2, pp. 97-105, Apr. 1995.

[23] L. M. Ferreira, G. S. Greeley, J. A. Johnson, and G. J. King, "Load transfer at the distal ulna following simulated distal radius fracture malalignment," *J*

Hand Surg Am, vol. 40, no. 2, pp. 217-223, Feb. 2015.

[24] J. D. Johnston, M. P. McDonald, and S. A. Kontulainen, "Off-axis loads cause failure of the distal radius at lower magnitudes than axial loads: A side-to-side experimental study," *J Orthop Res*, vol. 38, no. 8, pp. 1688-1692, Aug. 2020.

[25] G. Chang, et al., "Microstructural and mechanical properties of cortical and cancellous bone," *Journal of Biomechanics*, vol. 45, no. 12, pp. 1965-1972, 2012.

[26] J. E. Koivumäki, et al., "CT-based finite element models can predict proximal femur fractures," *Bone*, vol. 50, no. 5, pp. 1234-1241, 2012.

[27] E. A. Gomes, H. H. Diana, J. S. Oliveira, Y. T. Silva-Sousa, A. C. Faria, and R. F. Ribeiro, "Reliability of FEA on the results of mechanical properties of materials," *Braz Dent J*, vol. 26, no. 6, pp. 667-670, Nov.-Dec. 2015.

[28] M. R. Bosisio, M. Talmant, W. Skalli, P. Laugier, and D. Mitton, "Apparent Young's modulus of human radius using inverse finite-element method," *J Biomech*, vol. 40, no. 9, pp. 2022-2028, Nov. 2007.

[29] R. Boyer, G. Welsch, and E. W. Collings, *Materials Properties Handbook: Titanium Alloys*. Ohio: ASM International, 2007.

[30] D. M. Lichtman, R. R. Bindra, M. I. Boyer, M. D. Putnam, D. Ring, D. J. Slutsky, J. S. Taras, W. C. Watters, M. J. Goldberg, M. Keith, C. M. Turkelson, J. L. Wies, R. H. Haralson, K. M. Boyer, K. Hitchcock, and L. Raymond, "American Academy of Orthopaedic Surgeons clinical practice guidelines on the treatment of distal radius fractures," *JBJS*, vol. 93, no. 8, pp. 775-778, Apr. 2011.

[31] R. Zdero, S. Shah, M. Mosli, H. Bougherara, and E. H. Schemitsch, "The effect of the screw pull-out rate on cortical screw purchase in unreamed and reamed synthetic long bones," *Proc Inst Mech Eng H*, vol. 224, no. 3, pp. 503-513, 2010.

[32] *Standard Specification and Test Methods for Metallic Medical Bone Screws*, ASTM International.

[33] DASH Outcome Measure. [Online]. Available: https://www.iwh.on.ca/tools-and-guides/dash-outcome-measure [Accessed 6 September 2023].

[34] M. Viceconti, F. Pappalardo, B. Rodriguez, M. Horner, J. Bischoff, and T. F. Musuamba, "In silico trials: Verification, validation and uncertainty quantification of predictive models used in the regulatory evaluation of biomedical products," *Methods*, vol. 185, pp. 120-127, Jan. 2021.

[35] L. Obert, F. Loisel, N. Gasse, and D. Lepage, "Distal radius anatomy applied to the treatment of wrist fractures by plate: A review of recent literature," *SICOT J*, vol. 1, p. 1, Jun. 2015.

[36] K. Frydrýšek, G. Theisz, L. Bialy, L. Pliska, and L. Pleva, "Finite element modelling of T-plate for treatment of distal radius," *Intelligent Systems for Computer Modelling*, vol. 423, pp. 1- 10, 2016.

[37] F. Amirouche, and G. F. Solitro, "Challenges in modeling total knee arthroplasty and total hip replacement," *Procedia IUTAM*, vol. 2, pp. 18-25, May 2011.

[38] T. Topp, T. Müller, S. Huss, P. H. Kann, E. Weihe, S. Ruchholtz, and R. P. Zettl, "Embalmed and fresh frozen human bones in orthopedic cadaveric studies: Which bone is authentic and feasible? A mechanical study," *Acta Orthopaedica*, vol. 83, no. 5, pp. 543–547, 2012.

[39] C. Gluek, R. Zdero, and C. E. Quenneville, "Evaluating the mechanical response of novel synthetic femurs for representing osteoporotic bone," *Journal of Biomechanics*, vol. 111, p. 110018, 2020.

[40] S. Battula, A. J. Schoenfeld, V. Sahai, G. A. Vrabec, J. Tank, and G. O. Njus, "The effect of pilot hole size on the insertion torque and pullout strength of self-tapping cortical bone screws in osteoporotic bone," *Journal of Trauma and Acute Care Surgery*, vol. 64, no. 4, pp. 990–995, 2008.

[41] D. A. Benoit, F. Le Navéaux, A. Posch, and J. Clin, "Orthopedic screw pullout prediction: Validation of a virtual mechanical test for the prediction of screw pullout forces in Sawbones polyurethane foam in accordance with ASTM F543 standard," 2023.

[42] U. Liljenqvist, L. Hackenberg, T. Link, and H. Halm, "Pullout strength of pedicle screws versus pedicle and laminar hooks in the thoracic spine," *Acta Orthopaedica Belgica*, vol. 67, no. 2, pp. 157–163, 2001.

Wares Chancharoen was born on November 18th, 1989, in Bangkok, Thailand. He received the B.Eng. degree in mechanical engineering from King Mongkut's University of Technology Thonburi, Thailand, in 2012 and the M.Sc. and Ph.D. degrees in information science at Nagoya University, Japan. He is currently an Assistant Professor at Princess Srisavangavadhana Faculty of Medicine, Chulabhorn Royal Academy, Thailand. His research interests include space medicine, space engineering, mechanical engineering, and medical device design. In 2018, he was awarded the Emerging Space Leadership (ESL) from the International Astronautical Federation (IAF), France. In 2019, he received the recognition award from the Deep Space Food Challenge as one of the international teams around the world from phase 1, which was conducted by The National Aeronautics and Space Administration (NASA), the Canadian Space Agency (CSA) and the Methuselah foundation.

Saran Seehanam was born in Roi-Et, Thailand, in 1997. He received the B.Eng. and M.Eng. degrees in Mechanical engineering from King Mongkut's University of Technology Thonburi (KMUTT) in 2023. He worked as a research assistant at Osseo Lab, KMUTT from 2020-2023. He has been the research assistant with AIIM Laboratory at Chulabhorn Royal Academy since 2023. He is the author and co-author of 6 articles. His areas of interest in research are fluid mechanics, biomedical engineering, additive manufacturing, and space science.

Thanapon Chobpenthai was born in Kanchanaburi, Thailand, in 1985. Assistant Professor Dr. Thanapon Chobpenthai is a specialist in malignant bone tumors and sarcomas. He is currently serving at the Princess Srisavangavadhana Faculty of Medicine, Chulabhorn Royal Academy in Bangkok, Thailand. His primary areas of expertise are orthopedic surgery, particularly focused on bone tumors.

Dr. Chobpenthai has an extensive academic background and clinical experience. He completed his medical education and subsequent specialization at Lerdsin Hospital. He is involved in both teaching and research at the Chulabhorn Royal Academy, contributing to the academic community through various publications and editorial contributions in the field of orthopedic surgery and oncology.

Todsaporn Fuangrod was born in Uttaradit, Thailand, in 1983. He received the B.Eng. degree in Computer Engineering from King Mongkut's Institute of Technology Ladkrabang, Bangkok, in 2007 and M.Phil. in Medical Physics and Ph.D. in Electrical Engineering from The University of Newcastle, NSW, Australia, in 2012 and 2016, respectively. From 2016 to 2017, he was a Post-doctoral Fellow with the Department of Radiation Oncology at Calvary Mater Newcastle Hospital, Australia. Since 2017, he has been an Assistant Dean and Lecturer with the Princess Srisavangavadhana Faculty of Medicine, Chulabhorn Royal Academy, Thailand. His research interests include medical image processing, artificial intelligence, real-time dosimetry, and adaptive radiation therapy. Dr. Fuangrod has received several awards, including gold and silver medals at international invention exhibitions, and has published 23 articles and 30 conference proceedings and abstracts.

Chavin Jongwannasiri received D.Eng. degree in Systems Engineering from Nippon Institute of Technology, Japan, in 2016. He also received both the B.Eng. and M.Eng. in Mechanical Engineering from King Mongkut's University of Technology Thonburi, Thailand, in 2008 and 2010, respectively. He is currently an Assistant Professor at Princess Srisavangavadhana Faculty of Medicine, Chulabhorn Royal Academy. His research interests are biomechanics, biomedical engineering, and surface modification, especially cell culture reactions applied to dental and medical applications.